Geomorphology 273 (2016) 189–201

Contents lists available at ScienceDirect

Geomorphology

journal homepage: www.elsevier.com/locate/geomorph

Sensitivity of the sediment trapping capacity of an estuarine mangrove forest

P.W.J.M. Willemsen [a,*], E.M. Horstman [a,b], B.W. Borsje [a,c], D.A. Friess [d], C.M. Dohmen-Janssen [a]

[a] Water Engineering and Management, University of Twente, P.O. Box 217, 7500 AE Enschede, The Netherlands
[b] School of Science, University of Waikato, Private Bag 3105, Hamilton 3240, New Zealand
[c] Marine and Coastal Systems, Deltares, P.O. Box 177, 2600 MH Delft, The Netherlands
[d] Department of Geography, National University of Singapore, 1 Arts Link, Singapore 117570, Singapore

ARTICLE INFO

Article history:
Received 21 February 2016
Received in revised form 25 July 2016
Accepted 27 July 2016
Available online 29 July 2016

Keywords:
Mangrove resilience
Sediment starvation
Coastal squeeze
Sea-level rise
Observational-numerical study
Mangroves in urbanized areas

ABSTRACT

Intertidal mangrove forests exist in a dynamic coastal environment that is increasingly impacted by human interference, leading to habitat fragmentation, reduced habitat quality and changing hydrodynamic and geomorphological conditions. Biophysical feedback mechanisms are essential to maintain mangrove ecosystems under such changing conditions, for example by facilitating sediment deposition during periods of tidal flooding to allow for long-term coastal accretion. However, human interferences affect these biophysical interactions. This study investigated the consequences of two widespread anthropogenic intervention scenarios on biophysical interactions in mangroves: sediment starvation (reduced sediment supply) and coastal squeeze (limited landward accommodation space). Field observations of hydrodynamics and sediment dynamics were conducted in Mandai mangrove fringing the sheltered northern shore of Singapore. A process-based numerical model (Delft3D) of this field site was set-up, providing accurate approximations of the observed flow velocities and deposition rates. This model was used for a scenario analysis of the initial response of the sediment trapping capacity in the mangrove system to instantaneous changes related to anthropogenic interventions. This analysis showed increased deposition rates in major parts of the mangrove when sediment supplies increased (up to three times more deposition after 1 tide) or when the landward accommodation space of the mangrove was extended (+17% deposition). A comparison of the outcomes of these scenarios with the current state of the mangrove underlined a lack of short-term sediment trapping capacity, affecting the (longer-term) adaptive capacity of the system. Thus, at present Mandai mangrove is potentially affected by reduced sediment supply and limited landward accommodation space. Importantly, actions to reduce this anthropogenic influence could enhance mangroves' sediment trapping capacity, facilitating increased resilience to future projected changes such as sea-level rise. Understanding this influence of anthropogenic interventions on mangrove resilience is essential if we are aiming to maintain coastal ecosystem stability, especially along rapidly changing and urbanizing tropical shorelines.

1. Introduction

Intertidal mangrove forests provide multiple ecosystem services to coastal populations across the tropics and yet are highly threatened by anthropogenic interventions as tropical coastlines continue to develop rapidly. Conversion of mangroves for aquaculture, agriculture, urban development and subsistence use is causing a rapid decline in their extent (Duke et al., 2007; UNEP, 2014; Webb et al., 2014). Tidal wetlands such as mangroves are also threatened by long-term forcings such as sea-level rise (SLR), in conjunction with decreased sediment supply and reduced landward accommodation space (Thampanya et al., 2006; Kirwan and Megonigal, 2013; Krauss et al., 2014; Lovelock et al., 2015). Mangroves can potentially adapt to such forcings, and such forcings in conjunction with decreased sediment supply and reduced landward accommodation space, as long as species-specific physical and ecological thresholds are not exceeded. This species-specific resilience is facilitated by an array of biophysical interactions operating at a range of different temporal and spatial scales (Cahoon et al., 2006; Friess et al., 2012a).

A key biophysical feedback mechanism in coastal wetlands is the interaction between hydrodynamics (i.e. tidal flows and waves) and above-ground vegetation structures, and the subsequent impact on local geomorphology. Much of the research on coastal wetland biogeomorphology occurred in temperate saltmarshes in Europe and the US from the 1990s onwards, contributing to our understanding of how saltmarsh vegetation can reduce hydrodynamic energy due to breaking and frictional losses (Brampton, 1992; Leonard and Luther, 1995; Möller et al., 1999) and how such attenuation can contribute to

* Corresponding author.
E-mail address: p.willemsen@utwente.nl (P.W.J.M. Willemsen).

http://dx.doi.org/10.1016/j.geomorph.2016.07.038
0169-555X/

increased saltmarsh sedimentation (Leonard, 1997). However, while the above-ground vegetation may differ in saltmarshes (grasses and herbs) and mangroves (woody vegetation), they share similarities in their biogeomorphological processes and feedbacks due to their similar positions in the intertidal zone and similar vegetation establishment thresholds (Friess et al., 2012a). Thus, biogeomorphological principles derived from saltmarsh research may be applicable to mangrove systems, and vice versa biogeomorphological principles derived

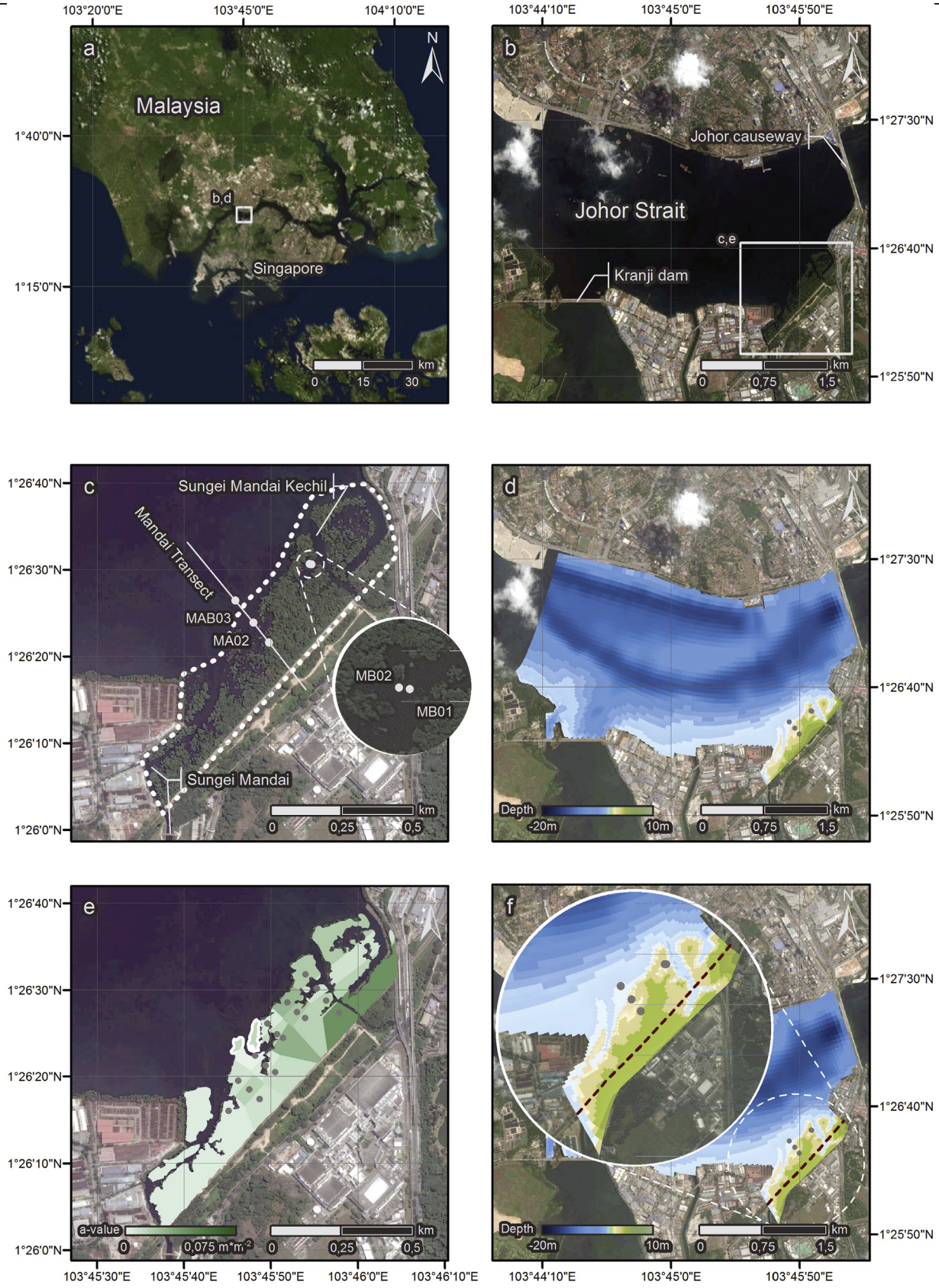

from mangrove studies can make important contributions to biogeomorphological paradigms.

Similar to saltmarshes, vegetation-attenuated hydrodynamics encourage sediment deposition in mangrove systems over the short-medium term (Horstman et al., 2015), and positive elevation changes over the longer term (Krauss et al., 2014), in conjunction with biogenic inputs such as organic matter production. Similar to saltmarshes, sediment deposition also increases in mangrove systems with a lower elevation with respect to mean sea level (van Wijnen and Bakker, 2001), as sediment deposition is facilitated during periods of tidal inundation (Kirwan and Megonigal, 2013). Increased sediment deposition and positive surface elevation change creates accommodation space for pioneer mangrove and saltmarsh vegetation to expand upon (Balke et al., 2011; Friess et al., 2012b), further enhancing their sediment trapping potential. These feedback loops are typical of ecosystem engineers that interact with their abiotic environment, changing it to their own benefit (Jones et al., 1994, 1997).

In mangroves, sediments can remain in suspension during flood tidal currents, due to the high micro-turbulence enhanced by the vegetation structures. The suspended sediments settle during slack tide when turbulence vanishes and the receding ebb tide is often too sluggish to resuspend these deposits (Furukawa and Wolanski, 1996). This sediment trapping capacity of mangroves depends on a range of biophysical feedback mechanisms and external forcings. The suspended sediment concentration (SSC) in the surrounding waters of mangroves is an important driver of the sediment accumulation in mangroves (Kirwan et al., 2010; Kirwan and Megonigal, 2013). In response to SLR, mangroves face an increased hydro-period, and hence an increasing sediment influx, potentially resulting in adapted biophysical feedbacks and enhanced sediment trapping (Mckee et al., 2007; Krauss et al., 2010). Previous studies observed accretion rates in mangroves that could offset the rate of SLR, provided that suspended sediment inputs are sufficient to sustain these accretion rates (e.g. Victor et al., 2004; Thampanya et al., 2006). However, the consequences of anthropogenic interventions are severely affecting fluvial sediment supply to the coastal zone, potentially resulting in reduced sediment supply to mangroves. Globally, reservoirs trap 26% of the total terrestrial sediment discharge, significantly reducing sediment inputs to downstream coastal systems (Syvitski et al., 2005). Hence, ongoing river damming has the potential to severely reduce the sediment trapping capacity of mangroves and their resilience to future SLR (Horstman et al., 2015; Lovelock et al., 2015).

Locations with substantial sedimentation have high success rates of natural mangrove establishment in minerogenic systems (Erftemeijer and Lewis III , 1999). Higher elevated intertidal areas have also been found to be more successful for mangrove and saltmarsh colonization (Wolters et al., 2005; Friess et al., 2012a). Hence, alleviation and removal of anthropogenic features, potentially blocking tidal exchange and accretion, can enhance mangrove establishment.

Coastal squeeze is another widespread impact (artificial or natural) that stresses coastal wetlands (Doody, 2004; Schleupner, 2008; Doody, 2013), such as mangroves. SLR requires mangroves to increase their surface elevation vertically (through sediment trapping or the addition of below-ground organic matter) and/or to move laterally inland to obtain an elevation gain that offsets the rate of SLR, so that the entire mangrove system maintains its relative position in the tidal frame (Cahoon et al., 2006). In cases where the inundation frequency and period of a mangrove increases and its landward migration space is limited, the mangrove is squeezed between the rising sea level and the artificial (e.g. fixed structure for coastal defense) or natural (topographic) landward boundary, leading to 'ecological drowning' (Friess et al., 2012a).

This study aims to address the biophysical interactions in estuarine mangroves in an urban environment by (I) obtaining field observations of the hydrodynamics and sediment dynamics in an estuarine mangrove affected by anthropogenic interventions; and (II) identifying the sensitivity of the sediment trapping capacity of estuarine mangroves as a consequence of such anthropogenic interventions. Field data were collected and have been used to calibrate and validate a numerical, process-based model (Delft3D) that was set-up to simulate hydrodynamics and sediment dynamics in the study area. The calibrated model was applied to analyze the sensitivity of the sediment trapping capacity of these estuarine mangroves in an urban environment, by simulating the initial response of the disturbed mangrove system to (instantaneous) changes of its sediment supply and landward accommodation space.

2. Methods

2.1. Study site

Mandai mangrove (1°26′21″N; 103°45′49″E, Fig. 1), located along the northern shores of Singapore, covers approximately 15.4 ha of intertidal area (Yee et al., 2010) and was once part of an extensive mangrove forest along Singapore's coast. Inland, Mandai mangrove is enclosed by the former Singapore-Malaysia railway and the rivers Sungei [Malay = river] Mandai (Besar) and Sungei Mandai Kechil, discharging into the area at the southwestern and northeastern side, respectively (Fig. 1b). Northeast of Mandai, the Johor causeway closes off the Straits of Johor and to the southwest an inland dam blocks the discharge from Sungei Kranji.

Mandai can be classified as a fringing mangrove forest (Mazda et al., 2007), situated in an estuary and exposed to semi-diurnal tides with a mean tidal range of approximately 2.6 m (3.9 m at spring tides). Wave exposure is very limited due to the limited fetch (<1000 m) in front of the mangrove. The vegetation at the seaward fringe primarily consists of the low elevation pioneer species *Avicennia alba* and *Sonneratia alba*. Further landward, the diverse back mangrove includes *Bruguiera cylindrica*, *B. gymnorrhiza*, *Excoecaria agallocha* and *Lumnitzera racemosa* (Friess et al., 2012c). The vegetation shows a fragmented and scattered pattern with an erosive trend with old trees at the mangrove fringe (Fig. 2a) and newly establishing seedlings and saplings in front of the mangrove (Fig. 2b).

2.2. Field data collection

Field data were collected in March and April 2015, at five different locations throughout the forest (Fig. 1c), providing a representative overview of the mangrove: location MA01 was situated in the elevated back of the mangrove forest vegetation; MA02 was located at the mangrove fringe within an extensive patch of recently established *Sonneratia* saplings; MAB03 was located at the intertidal mudflat; MB01 was positioned in a tidal creek discharging in the Sungei Mandai Kechil outlet and MB02 was located at the adjacent creek bank.

Fig. 1. (a) Singapore and Southern Malaysia surrounded by the Malacca Strait, Singapore Strait and the South China Sea. (b) The Straits of Johor with the Mandai mangrove. (c) Mandai mangrove including measurement locations and mangrove extent (dashed outline). (d) Bathymetry used in the Delft3D model (Kernkamp et al., 2005) overlying The Straits of Johor and Mandai mangrove. (e) Vegetation polygons in the model based on vegetation data available for locations marked by the gray dots (Lee, 2015). The vegetation density, quantified as average tree diameter [m] times average stem density [m^{-2}], is shown by the gradient (obtained through nearest-neighbor interpolation between measurement plots). The thick outlined polygons show the *Sonneratia* patches measured during the present study. (f) Extended model at the back of Mandai (south-east of the thick dashed line) for the scenario analysis. (Service layer credits panel a: Esri, DigitalGlobe, GeoEye, i-cubed, USDA, USGS, AEX, Getmapping, Aerogrid, IGN, IGP, swisstopo, and the GIS User Community. Service layer credits panels b–f: Google Earth).

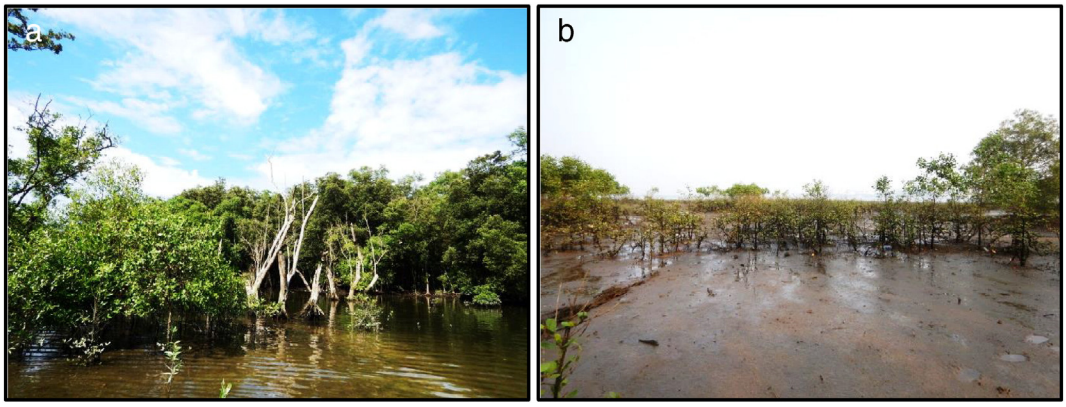

Fig. 2. (a) Fragmented and scattered pattern of vegetation at Mandai's mangrove fringe, including some old and dead trees. (b) *Sonneratia alba* sapling establishment in front of the mangrove.

2.2.1. Vegetation characteristics

An extensive vegetation survey was conducted in February and March 2015 by Lee (2015), wherein vegetation characteristics were measured within 17 circular plots with a radius of 7 m per plot (Fig. 1e; dots), over a total of five cross-shore transects. All mangrove trees within the plots exceeding 5 cm diameter at breast height (DBH, measured at a height of 1.30 m) were measured and their DBH and species were reported. In addition, saplings, representing all trees with a DBH smaller than 5 cm, were counted for all plots (Lee, 2015). It was assumed that the saplings in general had a diameter of 2.5 cm. An additional survey was conducted to measure individuals (<5 cm DBH) within a recently formed patch of *Sonneratia alba* saplings seaward of the mangrove forest. The outline of the patch was mapped with a GPS and the *Sonneratia* saplings (Fig. 2b) were sampled within a representative plot with a radius of 7 m. The stem diameter was measured at breast height. *Sonneratia* trees (five) within the same patch were sampled by measuring the diameter at the bed and at breast height. Due to the height of the vegetation at the study site, the canopy of the trees is not flooded and hence will not impact the hydrodynamics and sediment dynamics under regular conditions. Vegetation characteristics were averaged to obtain a single characteristic tree or sapling per plot. The measured plot with saplings was assumed representative for the mapped extent of the entire patch and the measured trees were extrapolated to the measured patch with *Sonneratia* trees.

2.2.2. Hydrodynamics

Hydrodynamics were mapped by monitoring flow velocities in horizontal (x, y) and vertical (z) directions, with Nortek Acoustic Doppler Velocimeters (ADVs). The ADV heads were mounted downward looking, measuring flow velocities at 0.07 m above the bed. A minimum water depth of approximately 0.25 m was required for data collection by the ADVs. To reduce flow disturbance, the mounting of the ADVs was oriented perpendicular to the prevailing flow directions of the tides. Probe heads were aligned to the north. The set-up of the ADVs was similar to the set-up used by Horstman et al. (2013). The sampling rate of the ADVs was 16 Hz, with 600 s per burst and a burst interval of 10 min.

Data was collected during multiple tidal cycles, with the instruments being deployed and retrieved at two subsequent low tides. Hydrodynamics at the back of the forest (MA01), the mangrove fringe (MA02) and the mudflat (MAB03, see Fig. 1c) were monitored during two near-spring high tides (24 March 2015 and 5 April 2015). Data were collected at the tidal creek (MB01), the tidal creek bank (MB02) and the mudflat (MAB03) during two different near-spring high tides (25 March 2015 and 6 April 2015). Flow velocities at location MAB03 were measured during all deployments, for reference.

The obtained hydrodynamic data were pre-processed using filtering, averaging and data correction procedures from Horstman et al. (2013). Inaccurate data were filtered by removing data with a mean correlation of the return signal below 80% (SonTek, 1997; Chanson et al., 2008). With the filtering procedure all irrelevant disturbances (e.g. due to shipping, animal activity or air bubbles) were removed. After filtering, data were averaged over the 10 min bursts to remove fluctuations caused by wind and swell waves. The filtering provided continuous data series for the monitored high tides.

2.2.3. Sediment deposition rates

Sediment deposition rates at Mandai were measured using 0.04 m^2 acrylic sediment traps, roughened with sandpaper to mimic the natural bottom roughness in the mangrove, comparable to the traps in Horstman et al. (2015). Traps were installed flush with the surrounding bed and secured with metal pins. Data were collected using three sediment traps at each of the locations in the back forest (MA01), the mangrove fringe (MA02), the tidal creek (MB01) and the tidal creek bank (MB02) during the respective deployments at these sites, whereas one sediment trap was deployed at the mudflat (MAB03) during all four periods. The sediment traps were rinsed separately with deionized water to collect the deposits. The dissolved deposits were filtered with pre-weighted filters (0.7 μm Whatman GF/F filters), which were dried in the oven (24 h at 105 °C) and weighted again. The replicated results per location were averaged and a standard deviation was defined.

In addition, sediment characteristics were analyzed for samples from the mobile top layer (<20 mm) at all measurement locations. Two undisturbed samples were retrieved from each location. Each sample was oven-dried (24 h at 105 °C) and lyophilized prior to a grain size analysis and an organic matter content analysis. Grain size analysis of

Table 1
Vegetation characteristics of the patch with *Sonneratia* saplings and of the patch with *Sonneratia* trees.

Patch	DBH [m]	Diameter bed [m]	Height [m]	Height of branching [m]	Diameter of branches [m]	Number of branches [–]	Surface [m^2]	Stem density [m^{-2}]
Saplings	–	0.036	1.120	0.121	0.029	1.66	4694	0.364
Trees	0.039	0.061	>2.0	>2.0	–	–	560	0.152

the dry sieved samples (2 mm mesh size) was performed with a particle size analyzer (Malvern Mastersizer 2000). The organic matter content was determined by the weight loss upon ashing of the dry sieved samples (4 h at 550 °C).

2.3. Model set-up

2.3.1. Model description

Similar to previous modeling efforts in mangroves and saltmarshes, this study applied the Delft3D software developed by Deltares (e.g. Temmerman et al., 2005; Horstman et al., 2015). The Delft3D-FLOW module solves the unsteady shallow-water equations in two (depth-averaged) or three dimensions. The system of equations consists of the horizontal momentum equations, the continuity equation, the sediment transport equation, and a turbulence closure (Lesser et al., 2004). The FLOW-module explicitly incorporates the drag and turbulence around rigid cylindrical plant structures in its 3D vegetation model (Deltares, 2015). Depth-averaged settings were applied for this study, since extensive test runs showed that the results of the depth-averaged model were similar to those of the 3D model (see also Hu et al., 2009; Horstman et al., 2015). In addition, the depth-averaged model run was executed within 8% of the time of a 3D model run (10 layers), allowing for a more comprehensive sensitivity analysis.

2.3.2. Model domain

The model domain consisted of Mandai mangrove and the surrounding section of the Straits of Johor (Fig. 1d). The model domain had a length of approximately 4.0 km (along the Straits) and a width of approximately 2.5 km (perpendicular to the Straits). The model grid and topography were part of the hydrodynamic Sungei Buloh Local Model (SBLM). The SBLM is nested in the Singapore Regional Model (SRM). The SRM has been developed to provide accurate tidal information in the Singapore Strait region (Kernkamp et al., 2005). The SRM has been extensively validated (e.g. Kurniawan et al., 2011) and was refined and aligned with recent depth contours by Hasan et al. (2012). The effect of grid resolution and nesting procedures on the prediction of tidal dynamics of Singapore's coastal waters is further studied by Hasan et al. (2016). Predicted water levels have previously been calibrated and validated rigorously for the SRM. The modeled flow velocities and currents of the SRM were compared by Hasan et al. (2016) with field data obtained at the southeast of Singapore in relative deep water. The model performance regarding the water level was expressed in the skill (0.98) and R^2 (0.94). The RMS for water levels was 0.70 and for flow velocities 0.39 (Hasan et al., 2016). The SBLM is a smaller scale, but more detailed version of the SRM, containing just the western part of the Straits of Johor. This model has been used successfully for predicting hydrodynamics in the nearby Sungei Buloh area (Kurniawan et al., 2014) and the local residence time of pollutants (Hasan et al., 2015). Water surface fluctuations computed with the SBLM showed good agreement with the field data. Only minor discrepancies existed, however these differences were within 10% (Kurniawan et al., 2014). In this study we applied the eastern end of the SBLM surrounding Mandai mangrove.

2.3.3. Topography, vegetation cover and bed roughness

The model extent was enclosed by the former Singapore-Malaysia railway and the Kranji Dam at the southern side, by the Johor Causeway at the eastern side and by the Malaysian embankment at the northern side. The model extent was subdivided in cells using a spherical curvilinear grid, taking the curvature of the earth into account (Fig. 1d). The grid cells were typically 10 m × 10 m in Mandai mangrove and gradually increased in size up to 50 m × 50 m in the Straits of Johor. The maximum elevation was equal to 4.00 m above MSL landward of the mangrove and the maximum depth was 16.67 m below MSL in the central areas of the Straits of Johor.

Vegetation characteristics from the field were standardized to densities per unit area and an average stem diameter per zone for representation in the vegetation model (Fig. 1e). The outline of the vegetation was determined using recent Google Imagery from 6 March 2015 (contemporary with the vegetation measurements). Vegetation characteristics from the nearest measurement plot were assigned to each grid cell within the outline of the mangrove vegetation, resulting in different vegetation zones. Additional vegetation patches observed in the field, beyond the vegetation outlines (white outlined patches Fig. 1e), were added to the model using three extra zones for which the obtained vegetation characteristics were also averaged (Table 1) and added to the vegetation model.

The applied bed roughness value has been obtained from the SBLM. A Manning bed roughness coefficient of 0.03 s $m^{-1/3}$ was assigned throughout the model domain (in x- and y-direction).

2.3.4. Hydrodynamic boundary condition

The model contained one open boundary in the Straits of Johor, at the western end of the model extent. The Sungei Mandai Besar and the Sungei Mandai Kechil (Fig. 1c) were both modeled as closed boundaries due to their very limited (under regular conditions) and controlled discharge. The water levels at the open boundary of the model were derived from a two-month model run of the SBLM nested in the SRM. The water levels from the SBLM at the location of the open boundary (midpoint of open boundary) of the present model were analyzed with the T-Tide Harmonic Analysis Toolbox (Pawlowicz et al., 2002). This analysis resulted in 33 tidal constituents with the dominant constituents being the semidiurnal M2 and S2 constituents and the diurnal O1 and K1 constituents (cf. Hasan et al., 2012). The full tidal spectrum was imposed as a boundary condition to the present model. A comparison of the two models, the SRM and the present model (with the imposed tidal boundary condition), showed that computed water levels near the Mandai mangrove were nearly equal ($R^2 = 0.99$).

2.3.5. Sediment dynamics

Sediment dynamics were not included in the SRM and SBLM and have been added to our model by assuming a uniform, cohesive, fine sediment (mud) with a constant settling velocity. The sandy fractions (Fig. 4) were neglected as the flow velocities in the study area were too small to transport (relevant amounts of) sand. Default values were used for the reference density and specific density of the mud: 1600 and 2650 kg m^{-3}, respectively (Deltares, 2015). The dry bed density was set to 1200 kg m^{-3}, and represents densities that are common for estuarine mud (Whitehouse et al., 2000).

The model was run with a fixed bed that could not erode, because the compacted and vegetated mangrove soil is less prone to erosion than the fresh deposits accumulated over the simulated tidal cycle. Moreover, little is known about the erosion thresholds of the bed material in mangroves (and in coastal wetlands in general). Hence, only freshly deposited sediments were allowed to be re-entrained, similar to the estuarine mangrove model of Horstman et al. (2015). In the absence of spatially explicit observations of the erosion parameter, the critical bed shear stress for erosion and the critical bed shear stress for sedimentation, these values were assumed to be uniform over the entire model domain. The critical bed shear stresses for erosion and sedimentation were set to, $5 \cdot 10^{-1}$ N m^{-2} and $1 \cdot 10^{3}$ N m^{-2}, respectively (Table 3). The erosion parameter was set to, $1 \cdot 10^{-4}$ kg m^{-2} s^{-1} (Table 3) (Deltares, 2015).

The boundary condition of the suspended sediment concentration (SSC) at the open boundary was specified using the data presented in Van Maren et al. (2014) for the east side of the Straits of Johor. The SSC inflow at the east side of the Johor causeway was estimated at an average of 150 mg l^{-1}. This value was assumed for the suspended sediment concentration at the open boundary of the present model. This value represented the intermediate conditions of the inter-monsoon

Table 2
Observed averaged sediment deposition rates and characteristic sediment properties at each of the monitoring locations in Mandai mangrove: back forest (MA01), mangrove fringe (MA02), mudflat (MAB03), creek bank (MB02) and creek (MB01).

Location	Deposition (standard deviation) [kg m^{-2}]	Mean grain size, D_{50} [μm]	Silt/clay fraction, <63 μm [%]	Organic matter [%]
Back forest	$2.69 \cdot 10^{-3}$ ($1.91 \cdot 10^{-3}$)	$3.83 \cdot 10^{2}$	10.97	2.94
Mangrove fringe	$4.50 \cdot 10^{-2}$ ($1.25 \cdot 10^{-2}$)	$4.40 \cdot 10^{1}$	64.94	15.21
Mudflat	$6.64 \cdot 10^{-2}$ ($4.29 \cdot 10^{-2}$)	$3.89 \cdot 10^{1}$	62.94	10.58
Creek bank	$4.34 \cdot 10^{-2}$ ($1.98 \cdot 10^{-2}$)	$2.73 \cdot 10^{1}$	70.42	15.74
Creek	$4.09 \cdot 10^{-2}$ ($1.95 \cdot 10^{-2}$)	$6.49 \cdot 10^{2}$	7.29	1.50

period between the wet season (December–January) and the dry season (June–July). Van Maren et al. (2014) described SSC values in the Johor Estuary of 10's of mg l^{-1} during low flow conditions, increasing to 1 g l^{-1} during extreme rainfall events.

The settling velocity of the modeled sediment fraction was based on data collected in the field (Table 2). In muddy environments, the settling velocity is not merely determined by the particle size, but also by flocculation, hindered settling, lag effects, etc. (Winterwerp, 2002; Van Maren and Winterwerp, 2012). Hence, it is impossible to define an exact settling velocity based on just the grain size distribution of fine sediments (clay and silt, Fig. 4). Flocculation of the fine-grained sediments, causing the settling velocity to increase, depends on the turbulent energy and sediment concentrations and hence results in spatially and temporally varying settling velocities (Van Maren and Winterwerp, 2012). Settling velocities of cohesive sediment in shallow tidal waters generally range between 0.1 and 1 mm s^{-1} (Wolanski et al., 1992; Van Maren and Winterwerp, 2012). In this study a settling velocity of 0.1 mm s^{-1} was adopted and this settling velocity was extensively varied for the sensitivity analysis (Section 3.2.2).

3. Results

3.1. Field observations

3.1.1. Vegetation

Vegetation characteristics obtained at the study site were normalized to densities per unit area. Vegetation densities ranged from 0.019 to 0.331 m^{-2}, with stem diameters ranging from 0.058 to 0.212 m (Fig. 1e). The number of saplings counted in the different plots ranged from 4 to 74 (Lee, 2015). The stem density of the surveyed *Sonneratia* patches with saplings (0.364 m^{-2}) was more than two times higher than the stem density of the patch with *Sonneratia* trees (0.152 m^{-2}; Table 1). The more mature *Sonneratia* trees had stem diameters (0.061 m) almost two times greater than the *Sonneratia* saplings (0.036 m). The saplings were branching close to the bed (Table 1) and were almost entirely covered with barnacles, significantly adding to the dimensions and rigidity of their stems and branches. The trees were similarly covered with barnacles, generally only below the high tide mark.

3.1.2. Hydrodynamics

Flow velocities measured in Mandai mangrove were generally lower than 10 cm s^{-1} (Fig. 3). The tidal in- and outflows within the forest and on the mudflat showed a clear asymmetry: a small velocity peak was observed during early flood tides and an extended period of sluggish flows was identified during subsequent ebb tides. On contrary, flow velocities within the creek showed a pronounced velocity peak on ebb tides, with velocities exceeding the incoming flood tides (cf. Horstman et al., 2013). The observations also showed a distinct decrease in the flow velocities from the front of the mangrove (mudflat; up to 0.07 m s^{-1}) to the higher elevated and denser vegetated back forest (up to 0.02 m s^{-1}) (Fig. 3).

3.1.3. Sediment dynamics

Sediment deposition showed a cross-shore decrease throughout the mangroves (Table 2), comparable to the gradient in flow velocities, with the largest deposition observed on the mudflat ($6.64 \cdot 10^{-2}$ kg m^{-2}). The deposition decreased to $2.69 \cdot 10^{-3}$ kg m^{-2} at the back of the mangrove. The standard deviation of the observed deposition rates was relatively large due to the variation in maximum water levels during the subsequent data collection periods, changing the tidal window for sediment deposition. In addition, some large particles were observed on the sediment traps and faunal activity might have affected our observations as well (by e.g. small snails, mud skippers and crabs).

Observed grain sizes of the top of the bed (<20 mm below the surface) at the mudflat, mangrove fringe and creek bank were quite similar, with 10–16% clay and silt (Fig. 4; Table 2). The sediment fractions at the

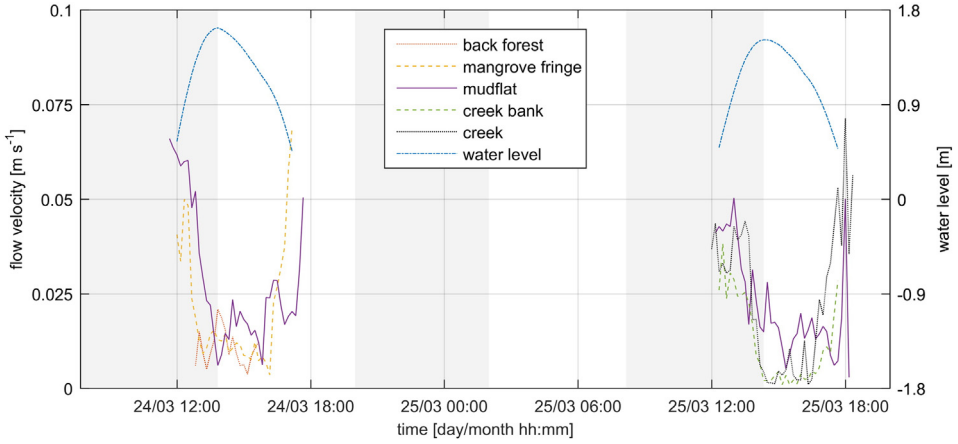

Fig. 3. Flow velocities and water levels as observed at the monitoring locations: back forest (MA01), mangrove fringe (MA02), mudflat (MAB03), creek bank (MB02) and within the creek (MB01).

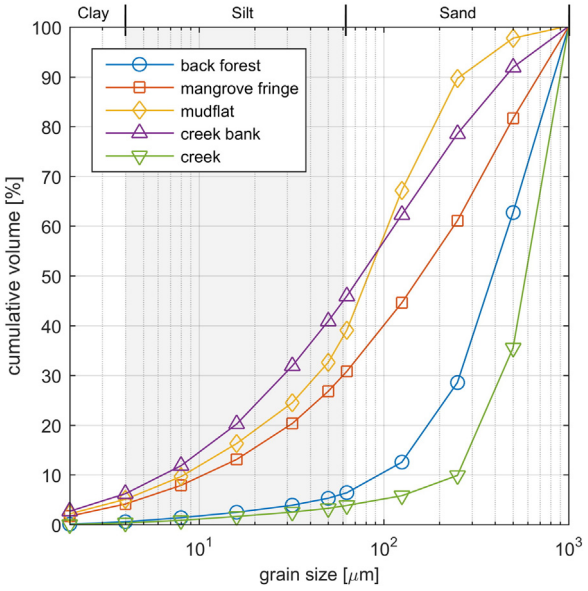

Fig. 4. Grain size distributions, defining the cumulative grain size fractions at the measurement locations: back forest (MA01), mangrove fringe (MA02), mudflat (MAB03), creek bank (MB02) and creek (MB01).

back of the mangrove and the creek were sandy; the silt/clay fractions were only 11 and 7.3%, respectively (Table 2). The mean grain size at the back of the mangrove was relatively large (383 μm). Bed material in the tidal creek was largely sandy (D_{50} = 649 μm), due to the concentrated flow and the related high flow velocities. The organic matter content (Table 3) was greatest in the center of the mangrove (mangrove fringe and creek bank), which was the most vegetated part of the site. The organic matter content of the mudflat and of the more exposed parts of the forest (mangrove fringe and creek bank) was comparable with data obtained in other mangrove studies (e.g. Horstman et al., 2015).

3.2. Model results

3.2.1. Calibration

The new model had to be calibrated in the eddy viscosity and eddy diffusivity, because of the switching from the 3D SBLM to a depth-averaged model. Those parameters should typically be in the range of 1 to 10 $m^2\ s^{-1}$ for grid cell dimensions of tens of meters or less and in the range of 10 to 100 $m^2\ s^{-1}$ for grid cell dimensions of hundreds of meters or more (Deltares, 2015). Both the eddy viscosity and diffusivity have been varied over the range of 1 to 25 $m^2\ s^{-1}$ (Table 3) for the model calibration.

The computed flow velocities and deposition rates, for a single tide in the period 24–25 March 2015, were compared with the observations in the field. Computed deposition rates, only comprising the fine sediments incorporated in the model, have been compared to the fine fractions (<63 μm) of the measured sediment deposition obtained by multiplying the deposition on the sediment traps with the fraction of fines obtained from the grain size distribution for the same location (Table 2). The correlation coefficient (R^2) is calculated for the comparison between the observed and computed velocities and deposition rates across all measurement locations.

An eddy diffusivity and viscosity of 14 $m^2\ s^{-1}$ resulted in the best agreement between the computed and observed flow velocities during these two days (Fig. 5) and for the computed and observed deposition during the spring high tide at the 24th of March (Fig. 6). The computed flow velocities compared favorable to the measured flow velocities, including the tidal asymmetry (R^2 = 0.37). Flow velocities were approximated best at the deeper inundated parts (mudflat and creek bank).The simulated deposition of fine sediments showed a highly accurate (spatial) match with the observations (Fig. 6; R^2 = 0.97).

3.2.2. Sensitivity analysis

To better understand the effect of any changes to the model parameters on the computed sediment dynamics, and to test the robustness of the model, a sensitivity analysis was conducted for the model parameters for which the assumed values were most uncertain. Those uncertain model parameters were the settling velocity, the erosion parameter, the critical bed shear stress for erosion and the critical bed shear stress for deposition. The values of these parameters were varied around their initial values (Table 3). The critical bed shear stress for deposition is only lowered, as its initial value was the upper limit.

Very minor changes (<0.01%) in the computed deposition rates were obtained for variations of the erosion parameter, the critical bed shear stress for erosion and the critical bed shear stress for deposition. The computed deposition rates were found to be more sensitive to variations in the settling velocity (Fig. 7). The variation in the computed deposition rates compared well with the variation in the deposition rates observed in the field at the forest fringe (MA02), at the mudflat (MAB03) and at the creek bank (MB02). The measured deposition at the back of the forest (MA01) was almost zero, whereas the range computed by the sensitivity analysis was higher (2.9–13 g m^{-2}). This could be explained by the relatively steep slope near measurement location MA01 at the back of the mangroves. The monitoring point is represented by a much larger grid cell in the model. This specific grid cell contains this slope, enhancing the deposition in the entire cell. In general, the variation of the predicted deposition rates, due to the uncertainty in the selected input parameters, resembled the variations in the observed values in the field. This finding corroborates that the model accurately represents the processes underlying the observed sediment dynamics and that the selected parameter values are within the actual ranges of the (unknown/uncertain) field conditions.

3.3. Sediment trapping capacity of mangroves

The calibrated model was used to simulate the initial response of the tidal-scale deposition in the mangroves for two scenarios; 1) an instantaneous increase of the suspended sediment concentrations in the Straits of Johor, i.e. alleviating the present reduced sediment supply; and 2) an increase of the mangrove's accommodation space by removal of existing landward barriers and adding an open basin at the back of

Table 3
Model parameter, implemented value for each parameter and the related ranges of values that have been used for the model calibration and sensitivity analysis.

Parameters	[Units]		Model value	Range calibration	Range sensitivity analysis
ν	[$m^2\ s^{-1}$]	Eddy viscosity	$1.4 \cdot 10^{1}$	$1.0 \cdot 10^{0}$–$2.5 \cdot 10^{1}$	–
D	[$m^2\ s^{-1}$]	Eddy diffusivity	$1.4 \cdot 10^{1}$	$1.0 \cdot 10^{0}$–$2.5 \cdot 10^{1}$	–
w_s	[mm s^{-1}]	Settling velocity	$1.0 \cdot 10^{-1}$	–	$4.0 \cdot 10^{-2}$–$2.5 \cdot 10^{-1}$
M	[kg $m^{-2}\ s^{-1}$]	Erosion parameter	$1.0 \cdot 10^{-4}$	–	$2.0 \cdot 10^{-5}$–$5.0 \cdot 10^{-4}$
$\tau_{cr,e}$	[N m^{-2}]	Critical bed shear stress for erosion	$5.0 \cdot 10^{-1}$	–	$2.5 \cdot 10^{-1}$–$7.5 \cdot 10^{-1}$
$\tau_{cr,d}$	[N m^{-2}]	Critical bed shear stress for deposition	$1.0 \cdot 10^{3}$	–	$1.5 \cdot 10^{-1}$–$1.0 \cdot 10^{3}$

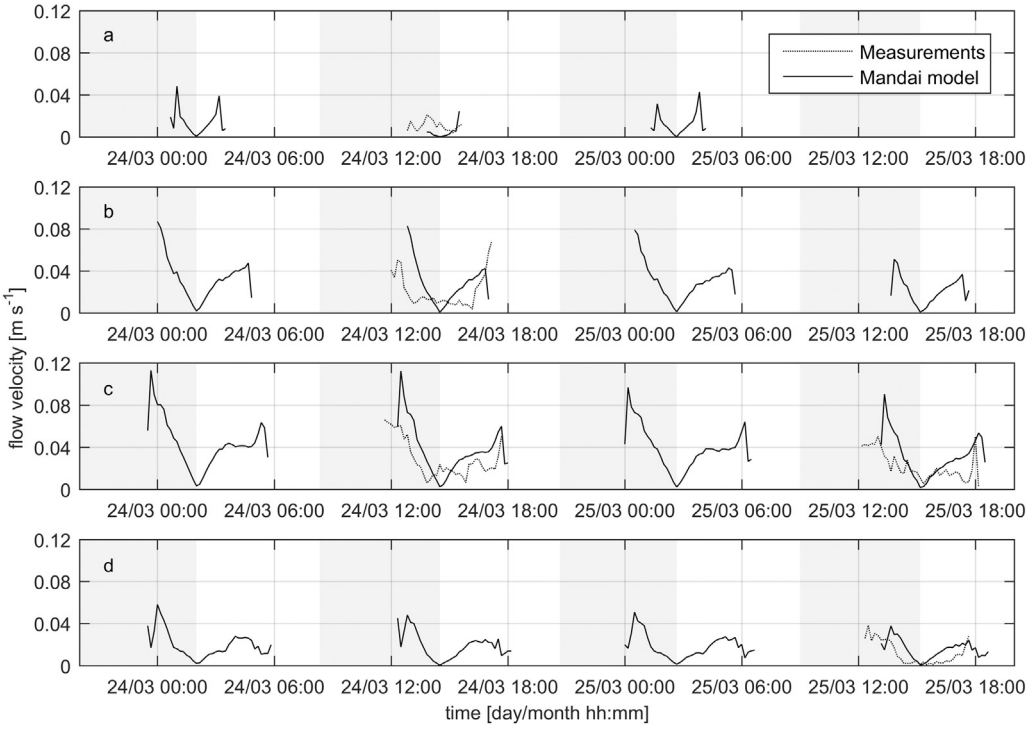

Fig. 5. Flow velocities measured in the field (dotted line) and computed with the calibrated model (continuous line) at (a) back forest (MA01), (b) forest fringe (MA02), (c) mudflat (MAB03) and (d) creek bank (MB02).

the forest. Both scenarios alleviate common mangrove stresses that reduce their adaptive capacity to SLR (Doody, 2004; Schleupner, 2008; Doody, 2013; Horstman et al., 2015; Lovelock et al., 2015). Initial system responses for both scenarios were simulated for a single tide (in the period 24–25 March), resulting in tidal-scale model predictions of the sediment deposition in the mangroves. These short-term model outcomes showed the initial impacts on the sediment trapping capacity of the mangroves if the interventions were relieved. This initial impact was used as an indicator for the longer-term effects that reduced sediment supply and limited landward accommodation space have on the adaptive capacity of these mangroves.

Additionally, to account for predicted future SLR, both scenarios were combined with a range of increasing mean sea levels (0.0–0.5 m), while the existing tidal amplitude was maintained. These simulations address the dependency between the instantaneous effects of mitigating, the abovementioned forcings and the actual mean sea level at the time of implementation.

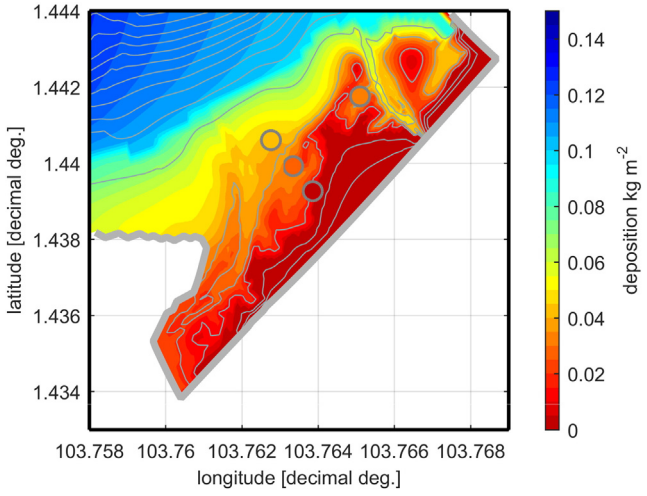

Fig. 6. Modeled and measured sediment deposition in Mandai mangrove. The color map shows the deposition of fine sediments computed with the model, while the fill color in the gray markers shows the measured average (over all measurements) deposition of fines. The depth is shown by the contour lines (1 m interval) on top of the modeled deposition.

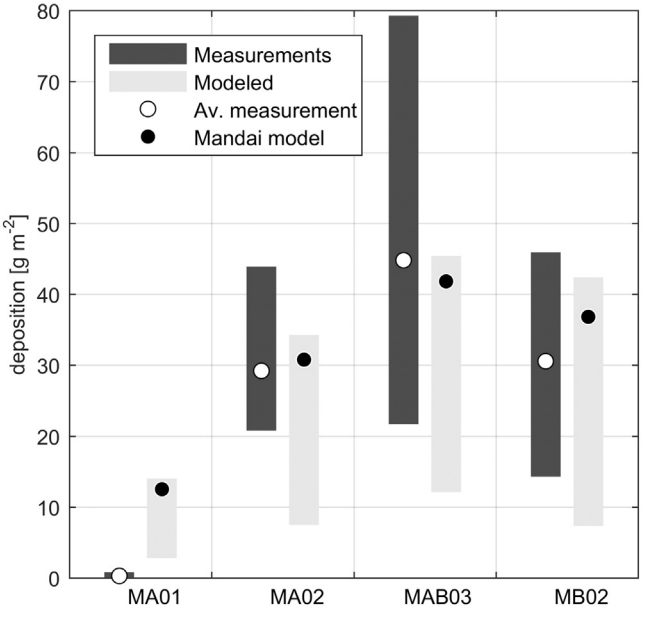

Fig. 7. Variation of the observed and computed deposition rates at four locations: back forest (MA01), forest fringe (MA02), mudflat (MAB03) and creek bank (MB02). The range of measured deposition (for all observations) is shown by the dark gray bars with the average deposition indicated by the white marker. The light gray bars show the range of modeled deposition rates computed in the sensitivity analysis, with the black marker showing the deposition for the calibrated model.

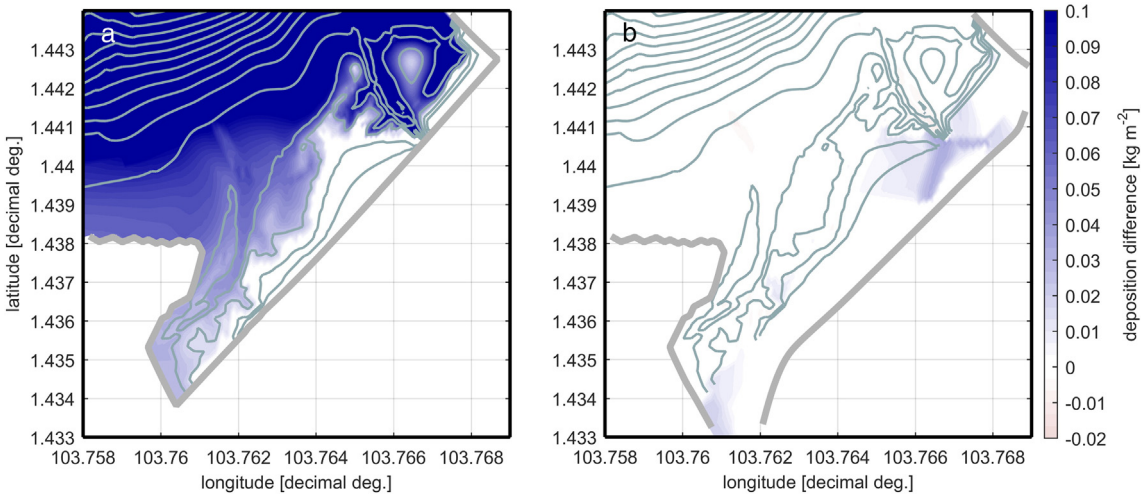

Fig. 8. Differential maps for the computed sedimentation compared to values computed with the original model for a single tide for: (a) a scenario with free exchange across the Johor Causeway and (b) a scenario with an open basin at the back of the mangrove.

3.3.1. Impacts of reduced sediment supply

The construction of the Johor causeway linking Singapore and Malaysia (Fig. 1b) in 1913 restricted tidal exchange between the western and eastern parts of the Straits of Johor (Friess et al., 2012c). For this scenario, the closure of the Straits was assumed to be one of the key causes of the reduced sediment supply to Mandai mangrove at present. The model set-up has been adapted for analyzing the influence of this reduced sediment supply: the Johor causeway was modified from a closed boundary to an open boundary, with astronomical forcing of the imposed water levels, similar to the boundary condition at the western open boundary (see Section 3.2.2). The new open boundary is closely located to the study site of Van Maren et al. (2014) where SSCs have been observed to be about 150 mg l^{-1} (0.15 kg m^{-3}). This value is imposed as a constant boundary condition for the SSC at the new open boundary (similar to the western open boundary condition).

The computed hydrodynamics for the situation with tidal exchange between the eastern and western parts of the Straits of Johor, with the present-day water levels, only showed minor deviations with respect to the original results. In general, the opening of the causeway resulted in increasing flow velocities in the mangrove during ebb tides, but differences were smaller than 0.01 m s^{-1}. Nevertheless, computed deposition rates increased consistently throughout the study site (Fig. 8a), with the increased deposition being inversely related to the height of the bed.

Simulated deposition rates were analyzed by aggregating the deposition per grid cell across three different zones: (I) the mangrove fringe, (II) the central mangrove and (III) the back of the mangrove (Fig. 9a). After the opening of the causeway, the deposition of fine sediments in the mangrove fringe and the central mangrove was >100% greater than the deposition under the current circumstances. The more dynamic mangrove fringe showed the greatest increase of the deposition rate with almost 300%. The computed sediment deposition also showed a progressive increase with increasing mean sea levels, with the sediment deposition showing greater increases when the re-opening of the Straits of Johor coincides with a higher mean sea level (Fig. 10a).

These results indicated that a reduced sediment supply did significantly reduce the sediment trapping capacity of the mangroves. Enabling tidal exchange across the causeway, increasing the sediment supply to the mangroves, resulted in deposition rates increasing with up to 300%. These results showed that re-establishing the sediment supply enhanced the resilience of the mangrove as higher deposition

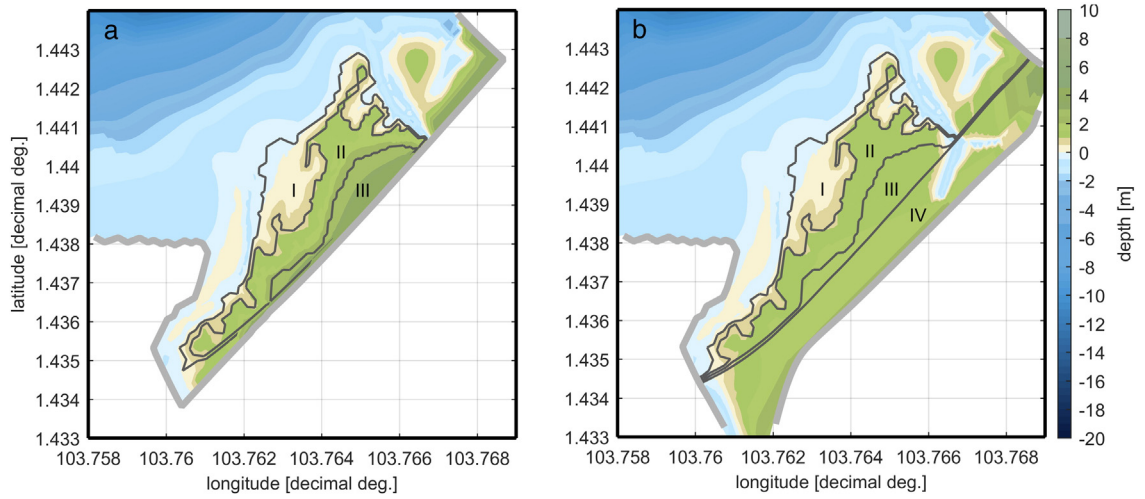

Fig. 9. Bathymetry of (a) the original model and (b) the extended model for the scenario regarding coastal squeeze. The contours indicate the boundaries of the characteristic zones within the mangrove: the fringe (I), the central mangrove (II) the back of the forest (III) and the extended basin at the back of the mangrove (IV).

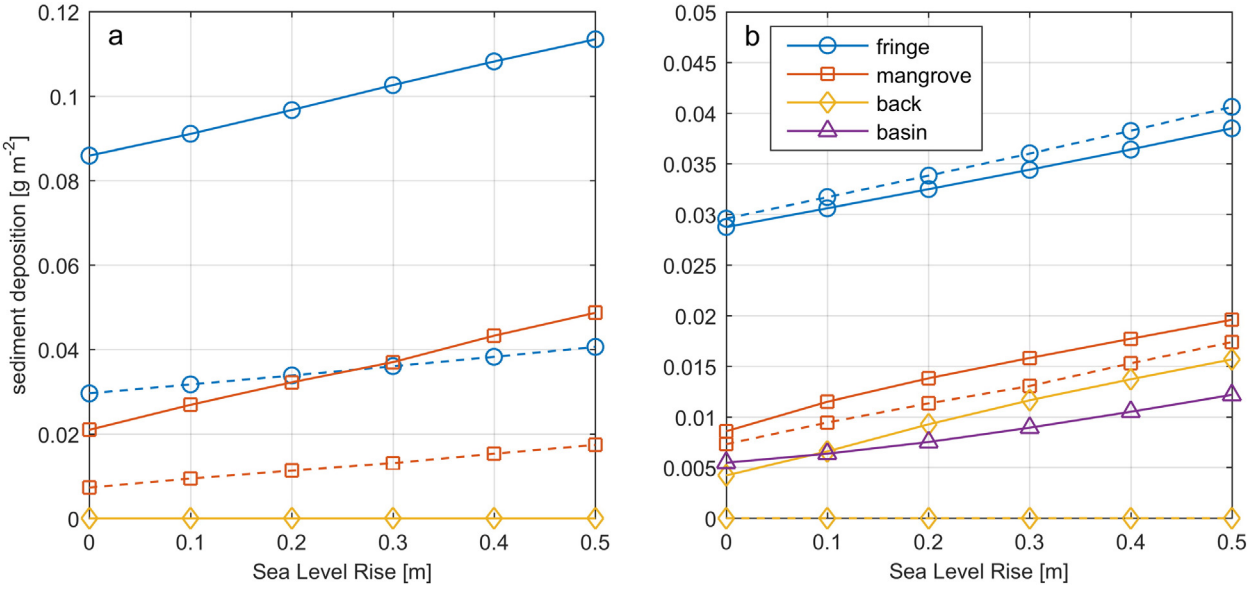

Fig. 10. Deposition of fine sediments within the characteristic zones of the mangrove for the original model (dashed lines) and for the scenarios with (continuous lines) for one tidal cycle. The sediment deposition in g m^{-2} is showed for (a) the scenarios with an open boundary imposed at the Johor Causeway and for (b) the scenario with an open basin at the back of the mangrove (note the different y-axis).

rates were found that showed a further increase with increased mean sea levels.

3.3.2. Impacts of limited accommodation space

The landward extent of the intertidal area at Mandai mangrove is currently suppressed by an embankment, which can cause coastal squeeze if combined with increasing water levels. To study the impact of this limitation of the accommodation space of the mangroves, the model was extended with an open basin landward of the mangroves (the back of the mangrove currently consists of grassland; Fig. 1f). Simultaneously, the bed level at the back of the mangrove was lowered from a maximum of +4.0 m MSL to +1.5 m MSL, as to facilitate tidal exchange within the basin. The elevation within the basin increased to +3.0 m and +4.0 m MSL at the eastern and western borders of the basin, respectively. The tidal creeks of the mangroves were extended into the basin, cutting through the new topography to enhance tidal exchange. The Manning roughness coefficient for the new basin was based on values for pasture and bare soil (just excavated) and the value was set to: 0.05 s m$^{-1/3}$ (Chow, 1959).

However, model outcomes showed an increasing tidal prism (volume of water flowing into and out of the mangrove) for simulations with the landward open basin. The tidal prism further increases with increasing mean sea levels. Flow velocities at the back forest (MA01) and within the mangrove fringe (MA02) were increasing. The increased flow velocities could be explained by the deeper inundated mangrove stretch not decelerating the flow as much as before and by the increased volume of water transported to and from the back of the mangrove.

Simulated deposition rates were analyzed similar to the scenario with an open boundary at the Johor Causeway, but with the new basin added as separate fourth zone (Fig. 9b). The deposition of fine sediments computed for this scenario (Fig. 10b; continuous lines) showed substantial differences with the original model (Fig. 10b; dashed lines). Deposition at the mangrove fringe showed a minor decrease (3–12%), due to the higher flow velocities, locally preventing the sediments to settle. However, the increased tidal prism transports more suspended sediments into the mangrove and to the back of the mangrove. Deposition in the central mangrove hence increased with approximately 17% (22% for a 0.2 m higher mean sea level; 13% for a 0.5 m higher mean sea level) and deposition in the back forest increased from 0 to 0.004 g m^{-2} (0 to 0.016 g m^{-2} with 0.5 m mean sea level increase). The computed deposition in all zones increased approximately linearly with increasing mean sea levels (Fig. 10b).

According to these results, the increasing mangrove extent resulted in a greater tidal prism, giving rise to higher flow velocities and greater sediment inputs into the mangroves. Although causing a slight reduction of the sediment deposition at the mangrove fringe, these increasing sediment inputs resulted in a substantial increase of the sediment deposition over the whole mangrove extent. The predicted deposition increased further for scenarios entailing an increase of the mean sea level. However, except for the back of the mangrove forest, where no deposition had been observed before, the sediment deposition with increasing mean sea levels was only marginally higher than the results prior to implementation of the basin (Fig. 10b).The computed increase of the deposition after implementation of the basin, especially in the back of the mangrove and in the new basin (Fig. 10b) provides the mangrove with better capabilities to maintain its position in the tidal frame, enhancing its resilience.

4. Discussion

4.1. Initial response versus long-term implications

Previous modeling studies have addressed the long-term morphodynamic development of mangroves (van Maanen et al., 2015) and saltmarshes (e.g. D'Alpaos et al., 2007; Kirwan and Murray, 2007) over decades to centuries. Key to those studies was the application of a simplified parameterization of the impact of vegetation on flow hydrodynamics through the drag coefficient, in combination with the application of a morphological factor to accelerate morphological developments and/or a simplified hydrodynamic model applying the Poisson hypothesis (i.e. friction balances water surface slopes). With timescales of morphological predictions overlapping with the developmental time scales of the vegetation, another key component of these models is the feedback between geomorphology and ecology, which is quantified according to various parameterizations (Fagherazzi et al., 2012; van Maanen et al., 2015). However, studies into these parameterizations are still in their infancy (Fagherazzi et al., 2012), potentially compromising the outcomes of these models. In addition, verifying these idealized models with reality is difficult due to lacking long-term and large-scale

data from the field and the inherent inability of the models to reproduce small-scale short-term observations (Coco et al., 2013).

In this study, we deployed a process-based model that accurately simulated short-term hydrodynamics and sediment dynamics at the study site. These short-term and small-scale dynamics feed directly into the longer-term and larger scale sediment dynamics of the mangroves (Cowell et al., 2003; Coco et al., 2013). Thereby, the process-based model predicted the initial response of the sediment trapping capacity of the mangrove system to instantaneous changes to its environmental settings due to anthropogenic interventions (cf. Horstman et al., 2015). This sensitivity analysis enhanced our understanding of the (short-term) contribution of these biogeophysical settings to the sediment trapping observed in the studied mangrove site and its (longer-term) adaptive capacity to past and future changes in these conditions.

The current model was only used for short-term simulations of conditions during which deposition was dominant. Wave action was limited in Mandai due to its sheltered location in the Straits of Johor and hence was neglected. Although extreme weather events can cause short-term erosion in wetlands (Aung et al., 2013; Krauss et al., 2014), this study focusses on the prevailing conditions and the restoring positive biophysical feedback mechanisms during relatively quiet conditions.

4.2. Hindcasts — the past impacts of anthropogenic interventions

Wetlands show resilient behavior to environmental changes like SLR by means of their intrinsic biophysical feedback mechanisms (e.g. Cahoon et al., 2006; Kirwan et al., 2016). However, these natural feedback mechanisms can be compromised by the consequences of anthropogenic interventions affecting their natural resilience (see Kirwan and Megonigal, 2013). Results of these interventions were observed in Mandai mangrove. Mature trees at the forest fringe were degrading, whereas *Sonneratia* seedlings have recently established on the mudflat. Mandai's fragmented mangrove vegetation could result in a loss of stabilizing feedback mechanisms hypothesized for mangrove and saltmarsh systems (Morris et al., 2002; Kirwan et al., 2010; Kirwan and Megonigal, 2013).

Data were collected to indicate the typical hydrodynamics and sediment dynamics during different periods of tidal flooding. Data were collected in March and April, being a period with average conditions. The wettest period appears in December–January and the driest in June–July (Van Maren et al., 2014). Flow velocities measured in Mandai during this study (both in a creek and in the forest) emphasized the consequences of anthropogenic interventions: flow velocities were significantly smaller than in studies of natural mangroves (Van Santen et al., 2007; Horstman, 2013; Horstman et al., 2015). These flow velocities were limited due to the blocking of longshore flows by the Johor causeway, and due to the very limited inland extent of the mangrove, limiting the tidal prism. Consequently, sediment deposition rates observed in Mandai were low compared to studies in less affected mangroves, e.g. Horstman et al. (2014), especially when taking into account that the data were collected during near-spring tides.

The sensitivity of the mangrove's sediment trapping capacity to reduced sediment supply was simulated by allowing water and sediment exchange across the currently closed Johor causeway (Fig. 1b). Second, the impact of the limited accommodation space was investigated by removing the landward embankments and modeling an open basin at the back of the mangrove. The computed instantaneous response of the mangrove showed a substantial increase of deposition for both scenarios: deposition throughout the mangrove increased when tidal exchange in the adjacent strait was re-established and when the basin was extended. In addition, the latter scenario activated the deposition at the back of the mangrove, enhancing the total sediment trapping in the mangrove.

The results of the present scenario analysis indicated that mangroves that have been exposed to anthropogenic interventions show increased sediment trapping capacity when reduced sediment supply is alleviated and when the accomodation space is increased. These effects were a clear indicator for the negative impacts that the reduced sediment supply and tidal prism have had on the stabilizing feedback mechanisms of Mandai mangrove. Such (past) effects may have had a significant and widespread effect on the present-day condition of many coastal wetlands. Worldwide, sediment influxes in coastal zones have decreased by 26% due to widespread river damming (Syvitski et al., 2005) and coastal zones have been prone to rapid urbanization.

4.3. Forecasts — the future consequences of anthropogenic interventions

Coastal squeeze is a widespread threat for mangroves, and coastal wetlands in general, due to the predicted rise of sea levels (Kirwan and Megonigal, 2013). Reduced landward accommodation space induced by human interferences such as land reclamation and coastal defense, decreases the natural dynamics of coastal wetlands (Pontee, 2013; Torio and Chmura, 2013). Combined with SLR, the reduced accommodation space gives rise to an accretionary deficit, ultimately resulting in coastal wetlands degradation (Kirwan et al., 2010). However, Doody (2013) states that larger habitats are more resilient to environmental perturbations and, provided the right environmental conditions, anthropogenically influenced saltmarshes can be restored.

The relatively small urban Mandai mangrove is constrained by a hard landward boundary at present, reducing the tidal exchange and thereby limiting sediment deposition throughout the mangroves. When the sea level rises, its limited sediment deposition rates are probably insufficient for the accretion to keep pace with the rising water level. Consequently, the recently settled vegetation at the mudflat is likely to drown (Kirwan et al., 2010). This drowning of the vegetation on the mudflat could potentially be followed by ecological drowning of the entire mangrove on the longer term. Extending the intertidal area with a basin at the back of the mangrove was found to result in increasing tidal dynamics and enhanced sediment deposition throughout the mangrove (Fig. 10). This increases the sediment trapping capacity, allowing the mangrove to better keep pace with SLR. Simultaneously, this strategy would allow the mangrove to migrate landward and potentially enhance vegetation establishment.

Biophysical feedbacks allow coastal wetlands to survive conditions under which they cannot develop (D'Alpaos et al., 2012; Kirwan and Megonigal, 2013). As quantitatively shown in this study, sufficient sediment input is a prerequisite for mangroves to increase their sediment trapping in the face of an increased sea level. Mitigating sediment starvation and/or reducing coastal squeeze was found to enhance the sediment supply to the mangrove and the subsequent trapping of these sediments in the mangrove. However, reduced sediment supply and landward embankments are typical features of coastal wetlands exposed to anthropogenic interventions (e.g. Coleman et al., 1998; Yang et al., 2006). Hence, the results of this study are believed to apply to many other mangroves around the world, in particular small urban mangroves.

5. Conclusions

This combined field and model study showed the impacts of anthropogenic interventions on the sediment trapping capacity in mangroves. Observations in the Mandai mangrove, an estuarine mangrove forest in an urban environment experiencing reduced sediment supply and constrained by landward embankments, showed that flow velocities and sediment deposition rates were limited compared to natural mangrove systems. At the same time, the mangrove vegetation was found to be rather fragmented and scattered.

An extensive scenario analysis with a field-verified hydrodynamic and sediment-dynamics model provided insight in the initial response of the mangrove when the reduced sediment supply and the limited accommodation space were mitigated. The model results predicted tidal-scale deposition rates within the mangrove to increase with up to 300% when sediment supplies were restored. In addition, sediment

deposition rates were found to show greater increases with an increase of the mean sea level when sediment supplies were restored. An extension of the landward accommodation space, simulated by removing the embankments behind the mangrove and extending the intertidal area in the inland direction, was found to result in increased flow velocities and enhanced deposition rates, mainly in the inner mangroves.

A comparison between these two scenarios and the current state of the Mandai mangrove indicated that the sediment trapping capacity of the mangroves is currently compromised by sediment starvation (reduced sediment supply) and coastal squeeze (limited landward accommodation space). Future SLR might threaten the survival of these and similar mangroves that face reduced sediment deposition due to the consequences of anthropogenic interventions, as enhanced deposition rates are paramount to keep up with the rising sea levels. Mitigating these human induced stresses was found to facilitate an increased sediment trapping capacity, enhancing the mangroves' adaptive capacity to future changes such as SLR. With sediment starvation and coastal squeeze being typical features of coastal wetlands exposed to anthropogenic interventions, these results may also apply to mangroves in other urbanized areas around the world.

Acknowledgements

This study was funded by the Royal Dutch Academy of Sciences' Academy Ecology Fund (UPS/375/Eco/J1514). Fieldwork was conducted under Singapore's National Parks Board permit NP/RP936. We acknowledge P. Taillardat, D. Richards, W. K. Lee (National University of Singapore) and C. Lyons for field assistance. We acknowledge W. K. Lee (National University of Singapore) for providing vegetation data. The Delft-3D model used in this study was provided by S.K. Ooi and S. Tay (National University of Singapore). L. van IJzerloo (Royal Netherlands Institute for Sea Research) is acknowledged for assistance with sediment analysis. B.W. Borsje was supported by the Netherlands Organization for Scientific Research (NWO-STW; 14363), E.M. Horstman was supported by The Royal Society of New Zealand's Marsden Fund (14-UOW-011) and P. W. J. M. Willemsen was supported by the research programme BE SAFE, financed primarily by the Netherlands Organization for Scientific Research (NWO; 850.13.012). Finally, we acknowledge the useful comments provided by two anonymous reviewers.

References

Aung, T.T., Mochida, Y., Than, M.M., 2013. Prediction of recovery pathways of cyclone-disturbed mangroves in the mega delta of Myanmar. For. Ecol. Manag. 293, 103–113. http://dx.doi.org/10.1016/j.foreco.2012.12.034.

Balke, T., Bouma, T.J., Horstman, E.M., Webb, E.L., Erftemeijer, P.L.A., Herman, P.M.J., 2011. Windows of opportunity: thresholds to mangrove seedling establishment on tidal flats. Mar. Ecol. Prog. Ser. 440, 1–9. http://dx.doi.org/10.3354/meps09364.

Brampton, A.H., 1992. Engineering significance of British saltmarshes. In: Allen, J.R.L., Pye, K. (Eds.), Saltmarshes: Morphodynamics, Conservation and Engineering Significance. Cambridge University Press, Cambridge, pp. 115–122.

Cahoon, D.R., Hensel, P.F., Spencer, T., Reed, D.J., McKee, K.L., Saintilan, N., 2006. Coastal wetland vulnerability to relative sea-level rise: wetland elevation trends and process controls. In: Verhoeven, J.A., Beltman, B., Bobbink, R., Whigham, D. (Eds.), Wetlands and Natural Resource Management vol. 190. Springer Berlin Heidelberg, pp. 271–292.

Chanson, H., Trevethan, M., Aoki, S., 2008. Acoustic Doppler Velocimetry (ADV) in small estuary: field experience and signal post-processing. Flow Meas. Instrum. 19 (5), 307–313. http://dx.doi.org/10.1016/j.flowmeasinst.2008.03.003.

Chow, V., 1959. Open Channel Hydraulics. McGraw-Hill, New York.

Coco, G., Zhou, Z., van Maanen, B., Olabarrieta, M., Tinoco, R., Townend, I., 2013. Morphodynamics of tidal networks: advances and challenges. Mar. Geol. 346, 1–16. http://dx.doi.org/10.1016/j.margeo.2013.08.005.

Coleman, J.M., Roberts, H.H., Stone, G.W., 1998. Mississippi river delta: an overview. J. Coast. Res. 14 (3), 698–716.

Cowell, P.J., Stive, M.J.F., Niedoroda, A.W., de Vriend, H.J., Swift, D.J.P., Kaminsky, G.M., Capobianco, M., 2003. The coastal-tract (part 1): a conceptual approach to aggregated modeling of low-order coastal change. J. Coast. Res. 19 (4), 812–827.

D'Alpaos, A., Lanzoni, S., Marani, M., Rinaldo, A., 2007. Landscape evolution in tidal embayments: modeling the interplay of erosion, sedimentation, and vegetation dynamics. J. Geophys. Res. Earth Surf. 112 (F1). http://dx.doi.org/10.1029/2006JF000537.

D'Alpaos, A., Da Lio, C., Marani, M., 2012. Biogeomorphology of tidal landforms: physical and biological processes shaping the tidal landscape. Ecohydrology 5 (5), 550–562. http://dx.doi.org/10.1002/eco.279.

Deltares, 2015. User Manual DELFT3D-FLOW.

Doody, J.P., 2004. 'Coastal squeeze'— an historical perspective. J. Coast. Conserv. 10 (1), 129–138. http://dx.doi.org/10.1652/1400-0350(2004)010[0129:CSAHP]2.0.CO;2.

Doody, J.P., 2013. Coastal squeeze and managed realignment in southeast England, does it tell us anything about the future? Ocean Coast. Manag. 79, 34–41. http://dx.doi.org/10.1016/j.ocecoaman.2012.05.008.

Duke, N.C., Meynecke, J.-O., Dittmann, S., Ellison, A.M., Anger, K., Berger, U., Cannicci, S., Diele, K., Ewel, K.C., Field, C.D., Koedam, N., Lee, S.Y., Marchand, C., Nordhaus, I., Dahdouh-Guebas, F., 2007. A world without mangroves? Science 317 (5834), 41–42. http://dx.doi.org/10.1126/science.317.5834.41b.

Erftemeijer, P.L.A., Lewis III, R.R., 1999. Planting mangroves on intertidal mudflats: habitat restoration or habitat conversion? Paper Presented at the ECOTONE-VIII Seminar, "Enhancing Coastal Ecosystem Restoration for the 21st Century". Ranong & Phuket

Fagherazzi, S., Kirwan, M.L., Mudd, S.M., Guntenspergen, G.R., Temmerman, S., D'Alpaos, A., Van De Koppel, J., Rybczyk, J.M., Reyes, E., Craft, C., Clough, J., 2012. Numerical models of salt marsh evolution: ecological, geomorphic, and climatic factors. Rev. Geophys. 50, 1–28. http://dx.doi.org/10.1029/2011RG000359.

Friess, D.A., Krauss, K.W., Horstman, E.M., Balke, T., Bouma, T.J., Galli, D., Webb, E.L., 2012a. Are all intertidal wetlands naturally created equal? Bottlenecks, thresholds and knowledge gaps to mangrove and saltmarsh ecosystems. Biol. Rev. 87, 346–366. http://dx.doi.org/10.1111/j.1469-185X.2011.00198.x.

Friess, D.A., Spencer, T., Smith, G.M., Möller, I., Brooks, S.M., Thomson, A.G., 2012b. Remote sensing of geomorphological and ecological change in response to saltmarsh managed realignment, The Wash, UK. Int. J. Appl. Earth Obs. Geoinf. 18, 57–68. http://dx.doi.org/10.1016/j.jag.2012.01.016.

Friess, D.A., Phelps, J., Leong, R.C., Lee, W.K., Wee, A.K.S., Sivasothi, N., Oh, R.R.Y., Webb, E.L., 2012c. Mandai mangrove, Singapore: lessons for the conservation of Southeast Asia's mangroves. Raffles Bull. Zool. (25), 55–65.

Furukawa, K., Wolanski, E., 1996. Sedimentation in mangrove forests. Mangrove Salt Marshes 1 (1), 3–10. http://dx.doi.org/10.1023/A:1025973426404.

Hasan, G.M.J., van Maren, D.S., Cheong, H.F., 2012. Improving hydrodynamic modeling of an estuary in a mixed tidal regime by grid refining and aligning. Ocean Dyn. 62 (3), 395–409. http://dx.doi.org/10.1007/s10236-011-0506-4.

Hasan, G.M.J., Kurniawan, A., Ooi, S.K., Hekstra, M., Broekema, Y., Bayen, S., 2015. Pollutants in mangrove ecosystems: a conceptual model for evaluating residence time. Paper Presented at the 5th International Conference on Water & Flood Management (ICWMF-2015), Dhaka, Bangladesh.

Hasan, G.M.J., van Maren, D.S., Ooi, S.K., 2016. Hydrodynamic modeling of Singapore's coastal waters: nesting and model accuracy. Ocean Model 97, 141–151. http://dx.doi.org/10.1016/j.ocemod.2015.09.002.

Horstman, E.M., 2013. Bio-Physical Interactions in Coastal Mangroves: Data Report — Field Campaign Trang, Thailand — Nov 2010/May 2011.

Horstman, E.M., Dohmen-Janssen, C.M., Hulscher, S.J.M.H., 2013. Flow routing in mangrove forests: a field study in Trang province, Thailand. Cont. Shelf Res. 71, 52–67. http://dx.doi.org/10.1016/j.csr.2013.10.002.

Horstman, E.M., Dohmen-Janssen, C.M., Narra, P.M.F., van den Berg, N.J.F., Siemerink, M., Hulscher, S.J.M.H., 2014. Wave attenuation in mangroves: a quantitative approach to field observations. Coast. Eng. 94, 47–62. http://dx.doi.org/10.1016/j.coastaleng.2014.08.005.

Horstman, E.M., Dohmen-Janssen, C.M., Bouma, T.J., Hulscher, S.J.M.H., 2015. Tidal-scale flow routing and sedimentation in mangrove forests: combining field data and numerical modelling. Geomorphology 228, 244–262. http://dx.doi.org/10.1016/j.geomorph.2014.08.011.

Hu, K., Ding, P., Wang, Z., Yang, S., 2009. A 2D/3D hydrodynamic and sediment transport model for the Yangtze Estuary, China. J. Mar. Syst. 77 (1–2), 114–136. http://dx.doi.org/10.1016/j.jmarsys.2008.11.014.

Jones, C.G., Lawton, J.H., Shachak, M., 1994. Organisms as ecosystem engineers. Oikos 69 (3), 373–386.

Jones, C.G., Lawton, J.H., Shachak, M., 1997. Positive and negative effects of organisms as physical ecosystem engineers. Ecology 78 (7), 1946–1957. http://dx.doi.org/10.1890/0012-9658(1997)078[1946:PANEOO]2.0.CO;2.

Kernkamp, H.W.J., Petit, H.A.H., Gerritsen, H., de Goede, E.D., 2005. A unified formulation for the three-dimensional shallow water equations using orthogonal co-ordinates: theory and application. Ocean Dyn. 55 (3–4), 351–369. http://dx.doi.org/10.1007/s10236-005-0017-2.

Kirwan, M.L., Megonigal, P., 2013. Tidal wetland stability in the face of human impacts and sea-level rise. Nature 504, 53–60. http://dx.doi.org/10.1038/nature12856.

Kirwan, M.L., Murray, A.B., 2007. A coupled geomorphic and ecological model of tidal marsh evolution. Proc. Natl. Acad. Sci. 104 (15), 6118–6122. http://dx.doi.org/10.1073/pnas.0700958104.

Kirwan, M.L., Guntenspergen, G.R., D'Alpaos, A., Morris, J.T., Mudd, S.M., Temmerman, S., 2010. Limits on the adaptability of coastal marshes to rising sea level. Geophys. Res. Lett. 37 (23). http://dx.doi.org/10.1029/2010GL045489.

Kirwan, M.L., Temmerman, S., Skeehan, E.E., Guntenspergen, G.R., Fagherazzi, S., 2016. Overestimation of marsh vulnerability to sea level rise. Nat. Clim. Chang. 6 (3), 253–260. http://dx.doi.org/10.1038/nclimate2909.

Krauss, K.W., Cahoon, D.R., Allen, J.A., Ewel, K.C., Lynch, J.C., Cormier, N., 2010. Surface elevation change and susceptibility of different mangrove zones to sea-level rise on pacific high islands of Micronesia. Ecosystems 13, 129–143. http://dx.doi.org/10.1007/s10021-009-9307-8.

Krauss, K.W., McKee, K.L., Lovelock, C.E., Cahoon, D.R., Saintilan, N., Reef, R., Chen, L., 2014. How mangrove forests adjust to rising sea level. New Phytol. 202 (1), 19–34. http://dx.doi.org/10.1111/nph.12605.

Kurniawan, A., Ooi, S.K., Hummel, S., Gerritsen, H., 2011. Sensitivity analysis of the tidal representation in Singapore Regional Waters in a data assimilation environment. Ocean Dyn. 61 (8), 1121–1136. http://dx.doi.org/10.1007/s10236-011-0415-6.
Kurniawan, A., Hasan, G.M.J., Ooi, S.K., Kit, L.W., Loh, L.L., Bayen, S., 2014. Understanding hydrodynamic flow characteristics in a model mangrove ecosystem in Singapore. APCBEE Procedia 10, 286–291. http://dx.doi.org/10.1016/j.apcbee.2014.10.054.
Lee, W. K. (2015). Unpublished data.
Leonard, L.A., 1997. Controls of sediment transport and deposition in an incised mainland marsh basin, southeastern North Carolina. Wetlands 17 (2), 263–274. http://dx.doi.org/10.1007/bf03161414.
Leonard, L.A., Luther, M.E., 1995. Flow hydrodynamics in tidal marsh canopies. Limnol. Oceanogr. 40 (8), 1474–1484. http://dx.doi.org/10.4319/lo.1995.40.8.1474.
Lesser, G.R., Roelvink, J.A., van Kester, J.A.T.M., Stelling, G.S., 2004. Development and validation of a three-dimensional morphological model. Coast. Eng. 51 (8–9), 883–915. http://dx.doi.org/10.1016/j.coastaleng.2004.07.014.
Lovelock, C.E., Cahoon, D.R., Friess, D.A., Guntenspergen, G.R., Krauss, K.W., Reef, R., Rogers, K., Saunders, M.L., Sidik, F., Swales, A., Saintilan, N., Thuyen, L.X., Triet, T., 2015. The vulnerability of Indo-Pacific mangrove forests to sea-level rise. Nature 526. http://dx.doi.org/10.1038/nature15538.
Mazda, Y., Wolanski, E., Ridd, P.V., 2007. The Role of Physical Processes in Mangrove Environments: Manual for the Preservation and Utilization of Mangrove Ecosystems. Terrapub.
Mckee, K.L., Cahoon, R.C., Feller, I.C., 2007. Caribbean mangroves adjust to rising sea level through biotic controls on change in soil elevation. Glob. Ecol. Biogeogr. 16 (5), 545–556. http://dx.doi.org/10.1111/j.1466-8238.2007.00317.x.
Möller, I., Spencer, T., French, J.R., Leggett, D.J., Dixon, M., 1999. Wave transformation over salt marshes: a field and numerical modelling study from North Norfolk, England. Estuar. Coast. Shelf Sci. 49 (3), 411–426. http://dx.doi.org/10.1006/ecss.1999.0509.
Morris, J.T., Sundareshwar, P.V., Nietch, C.T., Kjerfve, B., Cahoon, D.R., 2002. Responses of coastal wetlands to rising sea level. Ecology 83 (10), 2869–2877. http://dx.doi.org/10.1890/0012–9658(2002)083[2869:ROCWTR]2.0.CO;2.
Pawlowicz, R., Beardsley, B., Lentz, S., 2002. Classical tidal harmonic analysis including error estimates in Matlab using T_TIDE. Comput. Geosci. 28, 929–937. http://dx.doi.org/10.1016/S0098-3004(02)00013–4.
Pontee, N., 2013. Defining coastal squeeze: a discussion. Ocean Coast. Manag. 84, 204–207. http://dx.doi.org/10.1016/j.ocecoaman.2013.07.010.
Schleupner, C., 2008. Evaluation of coastal squeeze and its consequences for the Caribbean island Martinique. Ocean Coast. Manag. 51 (5), 383–390. http://dx.doi.org/10.1016/j.ocecoaman.2008.01.008.
SonTek, 1997. Pulse Coherent Doppler Processing and the ADV Correlation Coefficient.
Syvitski, J.P.M., Vörösmarty, C.J., Kettner, A.J., Green, P., 2005. Impact of humans on the flux of terrestrial sediment to the global coastal ocean. Science 308 (5720), 376–380. http://dx.doi.org/10.1126/science.1109454.
Temmerman, S., Bouma, T.J., Govers, G., Wang, Z.B., De Vries, M.B., Herman, P.M.J., 2005. Impact of vegetation on flow routing and sedimentation patterns: three-dimensional modeling for a tidal marsh. J. Geophys. Res. Earth Surf. 110 (F4), F04019. http://dx.doi.org/10.1029/2005JF000301.
Thampanya, U., Vermaat, J.E., Sinsakul, S., Panapitukkul, N., 2006. Coastal erosion and mangrove progradation of Southern Thailand. Estuar. Coast. Shelf Sci. 68 (1–2), 75–85. http://dx.doi.org/10.1016/j.ecss.2006.01.011.
Torio, D.D., Chmura, G.L., 2013. Assessing coastal squeeze of tidal wetlands. J. Coast. Res. 1049–1061 http://dx.doi.org/10.2112/JCOASTRES-D-12-00162.1.
UNEP, 2014. The Importance of Mangroves to People: A Call to Action.
van Maanen, B., Coco, G., Bryan, K.R., 2015. On the ecogeomorphological feedbacks that control tidal channel network evolution in a sandy mangrove setting. Proc. R. Soc. Lond. A 471 (2180). http://dx.doi.org/10.1098/rspa.2015.0115.
Van Maren, D.S., Winterwerp, J.C., 2012. The role of flow assymetry and mud properties on tidal flat sedimentation. Cont. Shelf Res. 60, S71–S84. http://dx.doi.org/10.1016/j.csr.2012.07.010.
Van Maren, D.S., Liew, S.C., Hasan, G.M.J., 2014. The role of terrestrial sediment on turbidity near Singapore's coral reefs. Cont. Shelf Res. 76, 75–88. http://dx.doi.org/10.1016/j.csr.2013.12.001.
Van Santen, P., Augustinus, P.G.E.F., Janssen-Stelder, B.M., Quartel, S., Tri, N.H., 2007. Sedimentation in an estuarine mangrove system. J. Asian Earth Sci. 29 (4), 566–575. http://dx.doi.org/10.1016/j.jseaes.2006.05.011.
van Wijnen, H.J., Bakker, J.P., 2001. Long-term surface elevation change in salt marshes: a prediction of marsh response to future sea-level rise. Estuar. Coast. Shelf Sci. 52 (3), 381–390. http://dx.doi.org/10.1006/ecss.2000.0744.
Victor, S., Golbuu, Y., Wolanski, E., Richmond, R.H., 2004. Fine sediment trapping in two mangrove-fringed estuaries exposed to contrasting land-use intensity, Palau, Micronesia. Wetl. Ecol. Manag. 12 (4), 277–283. http://dx.doi.org/10.1007/s11273-005-8319-1.
Webb, E.L., Jachowski, N.R.A., Phelps, J., Friess, D.A., Than, M.M., Ziegler, A.D., 2014. Deforestation in the Ayeyarwady Delta and the conservation implications of an internationally-engaged Myanmar. Glob. Environ. Chang. 24, 321–333. http://dx.doi.org/10.1016/j.gloenvcha.2013.10.007.
Whitehouse, R.J.S., Soulsby, R., Roberts, W., Mitchener, H., 2000. Dynamics of Estuarine Muds. Thomas Telfort Ltd. and HR Wallingford.
Winterwerp, J.C., 2002. On the flocculation and settling velocity of estuarine mud. Cont. Shelf Res. 22, 1339–1360. http://dx.doi.org/10.1016/S0278-4343(02)00010–9.
Wolanski, E., Gibbs, R.J., Mazda, Y., Mehta, A., King, B., 1992. The role of turbulence in the settling of mud flocs. J. Coast. Res. 8, 35–46.
Wolters, M., Garbutt, A., Bakker, J.P., 2005. Plant colonization after managed realignment: the relative importance of diaspore dispersal. J. Appl. Ecol. 42 (4), 770–777. http://dx.doi.org/10.1111/j.1365-2664.2005.01051.x.
Yang, S.L., Li, M., Dai, S.B., Liu, Z., Zhang, J., Ding, P.X., 2006. Drastic decrease in sediment supply from the Yangtze River and its challenge to coastal wetland management. Geophys. Res. Lett. 33 (6), 1–4. http://dx.doi.org/10.1029/2005GL025507.
Yee, A.T.K., Ang, W.F., Teo, S., Liew, S.C., Tan, H.T.W., 2010. The present extent of mangrove forests in Singapore. Nat. Singap. 3, 139–145.